Two-electron excitations in atomic calcium. III. High-lying resonances above the 4p threshold

Longhuan Kim and Chris H. Greene
Department of Physics and Astronomy, Louisiana State University, Baton Rouge, Louisiana 70803
(Received 25 January 1988)

A theoretical prediction of the photoionization spectrum of atomic calcium from the 4p threshold up to nearly the 6s threshold is obtained by an eigenchannel R-matrix calculation of the final-state multichannel quantum-defect parameters in LS coupling. The calculation shows how strong interactions are distributed among a large number (10–16) of channels and predicts an intricate spectrum of overlapping Rydberg series. Further calculations show that the $^1P^0$ Wannier-ridge states up to $11s11p$ obey a two-electron Rydberg formula, but that they are unusually difficult to excite directly from the ground state.

I. INTRODUCTION

In recent years steady progress has been made in the study of calcium photoabsorption both theoretically and experimentally.[1–9] The highest-resolution measurement of the calcium spectrum between the 4s and the 3d thresholds was given by Newsom.[1] At energies between the 3d and 4P thresholds, the experiment of Connerade *et al.*[3] was the best until very recently.[9] A number of theoretical calculations achieving various levels of agreement with these experiments have been reported.

Recently we published two papers on two-electron excitations in atomic calcium.[10,11] The first paper,[10] referred to as paper I hereafter, accounted for the dominant experimental spectral features up to the $Ca^+(4p)$ threshold. Paper I treated the two valence electrons of calcium in LS coupling. A small-scale eigenchannel R-matrix calculation[12–14] described the excitation dynamics in terms of a short-range reaction matrix. Standard multichannel quantum defect theory (MQDT)[15–17] was then used to calculate physical observables such as the photoionization cross sections. Excellent agreement was obtained between the length and velocity results for the cross sections, and good agreement with experiment was also achieved in that calculation. A second paper,[11] referred to as paper II below, used a geometrical transformation to describe effects of the spin-orbit interaction, including additional narrow resonances coupled to the final state by the spin-orbit interaction and also the photoelectron angular distribution and ionic alignment. In paper II the agreement with the experiment is markedly improved by including fine-structure effects. Nevertheless, paper II shows a noticeable discrepancy between the calculated cross section and the 1982 experiment of Connerade *et al.*[3] A very recent measurement by the same group has now eliminated virtually all of these discrepancies.[9]

The present work extends our calculation to provide a theoretical prediction of the photoionization spectrum of atomic calcium at higher energies still, from the 4p threshold up to nearly the 6s threshold. This energy range shows numerous multichannel Rydberg spectra of striking complexity, and includes several of the lower-lying Wannier-ridge-type states.[18–20]

In fact a major goal is to explore the properties of these ridge states and compare them to the better-known states of helium. Using our R-matrix procedure we identify the $5s5p$ and $6s6p$ autoionizing levels, analogs of the lowest $+$ states[21] that dominate the spectrum of helium.[22,23] For reasons not fully understood these play an unexpectedly minor role in the photoabsorption spectrum of calcium. (See Secs. III A and III C.) It appears that resonances such as $4d5p$ and $4d4f$ are much stronger than $5s5p$ and play the role of $+$-type states for calcium. In addition we have complemented our R-matrix calculation of the $5s5p$ and $6s6p$ levels by a more straightforward diagonalization procedure to predict level positions up to the $11s11p$ state. This procedure cannot easily predict the width or strength of these high-lying states. It does show, however, that the *nsnp* series of autoionizing ridge states obeys the same modified two-electron Rydberg formula which describes helium level positions so accurately. We are not aware of any measurement of the calcium spectrum in this energy range, and hope that our present work will stimulate efforts in this direction.

The method of calculation used in this paper is basically the same as the one used in papers I and II. However, it is not just a trivial extension of our previous work. Because of the higher energy range, much larger reaction volume, greater number of basis functions, and much larger number of open and weakly closed channels, several new problems arise. For these reasons this study sheds new light on fundamental aspects of R-matrix and multichannel quantum defect technologies. We take this opportunity to examine the growing energy dependence of the smooth, short-range parameters of MQDT in the presence of a large number of strongly interacting channels.

II. METHOD OF CALCULATION

A number of studies using a noniterative reformulation of the eigenchannel R-matrix calculation in conjunction with MQDT have been reported previously.[24–27] The theoretical background and details of implementation are

discussed in these references. We focus the present discussion on aspects especially relevant at high energies, where the large number of channel-interaction parameters poses some additional problems.

The calculation is performed in two distinct steps: a variational R-matrix calculation followed by an MQDT calculation. The first step obtains a short-range reaction matrix K_{ij} and dipole matrix elements for each eigenchannel. Reaction matrix eigenquantum defects μ_α and a matrix of eigenvectors $U_{i\alpha}$ are then obtained by diagonalizing K_{ij}. These dynamical parameters are all energy dependent and are calculated at selected energies to provide benchmark data for interpolation. The second step is a standard MQDT calculation on an arbitrarily fine energy mesh using the interpolated MQDT parameters. A common approach used frequently in MQDT calculations[28–30] starts with a set of short-range MQDT parameters which have been fitted to the observed spectrum in a certain energy range so as to reproduce experimental results. Such calculations normally assume these parameters to be energy independent, or else to have a simple (e.g., linear) energy dependence over some spectral range. As we have demonstrated in papers I and II, these assumptions are not valid over a wide energy range. At the higher energies considered in the present study, these short-range parameters acquire an energy dependence which is more complicated than at lower energies. One major aim of our calculation is to document this growing energy dependence as the excitation energy increases and as the number of channels increases. It should be stressed, however, that the short-range MQDT parameters remain simpler and smoother than the intricate multichannel Rydberg spectrum which we predict.

We treat the energy range from $E=-0.32$ to -0.12 a.u., measured relative to the threshold for two-electron escape. This range is extremely broad in the sense that it covers four different ionization thresholds $5s$, $4d$, $5p$, and $4f$, and the number of open channels increases from 5 to 12 as the energy varies from the lower end to the higher end of this range. It is preferable not to use a fixed number of channels for the entire energy range because of reasons considered in Sec. II D. Therefore we divide the energy range into several subregions and perform the calculation separately for each subregion using an appropriate number of variational trial functions and ionization channels.

The R-matrix calculation is done within a finite volume of configuration space called the reaction volume. The variational basis for the calculation consists of a series of two-electron configurations of the form $nln'l'$ for all possible excitation channels. Each basis function is an antisymmetrized product of two independent-particle wave functions, numerical eigenfunctions of the one-electron e-Ca^{2+} Schrödinger equation. The spin and angular functions are, of course, coupled to form a definite spin (S) and orbital angular momentum (L). The number of basis functions used for different subregions varies slightly depending on the number of open and weakly closed channels used in that subregion.

Next we turn to some new features encountered in the course of this calculation.

A. Binding energies of Ca^+

A good description of the e-Ca^{2+} interaction is very important for our calculation as the one-electron potential dictates the phase of a valence electron orbital emerging from the closed-shell ionic core. The detailed correlations between the two electrons outside this core depend sensitively on these phases. It is, therefore, important to find a potential which can reproduce the experimental one-electron energy levels of Ca^+. We have used in papers I and II a potential consisting of a screening term and of an empirical core-polarization term:

$$v_l(r)=v_l^{\mathrm{HS}}(r)-\frac{\alpha_{\mathrm{CP}}}{2r^4}\{1-\exp[-(r/r_{cl})^6]\}\ . \tag{1}$$

The screening term v_l^{HS} is obtained from a standard Hartree-Slater program.[31] The core polarization α_{CP} and the l-dependent cutoff radius r_{cl} are adjusted to obtain optimum agreement with the known spectrum of Ca^+. The values of α_{CP} and r_{cl} used in paper I produce excellent s and p energy levels. However, the $4d$ and $5d$ levels are a little too low when we utilize the value of r_{cl} optimized for the $3d$ level. For the low-energy spectrum treated in papers I and II, this is adequate but for the higher energies considered here we have readjusted the two parameters to obtain better $4d$ and $5d$ energy levels. The new values are $\alpha_{\mathrm{CP}}=6.8$, $r_{c0}=2.15$, $r_{c1}=2.75$, and for $l\geq 2$, $r_{cl}=1.835$. There is a misprint in Eq. (2) of paper I. The exponent 6 should lie outside the curly brackets like the one found in Ref. 32. However, in the present study we use the equation with the exponent inside the square brackets, exactly as written in paper I and in Eq. (1) above.

B. Basis functions and photoionization channels

The variational R-matrix calculation requires the determination of Hamiltonian matrix elements and the solution of the generalized eigenvalue problem:

$$\underline{\Gamma}C=b\underline{\Lambda}C\ . \tag{2}$$

The time needed to calculate the elements of $\underline{\Gamma}$ and $\underline{\Lambda}$ increases as the square of the number of basis functions, while the time required to solve Eq. (2) at each desired energy E increases as the cube of the number of basis functions. Clearly it is important to keep the basis set as small as possible. Explicit expressions for $\underline{\Gamma}$ and $\underline{\Lambda}$ can be found in Refs. 10 and 25–27.

Each basis function can be labeled as $nln'l'$, where n and l are the principal quantum number and the angular momentum quantum number of the inner electron and n' and l' are the quantum numbers of the outer electron. These basis functions can be divided into several groups according to the quantum numbers n,l,l', e.g., $4sn'p$, $3dn'f$, etc. which define the ionization channels of MQDT. The radial wave function for the second electron in each basis function is one of two types, either the "closed type" or the "open type." Open-type wave functions for the second electron are nonzero at the boundary of the reaction volume ($r=r_0$), while the closed-type orbitals vanish at r_0. For any particular channel to be

treated as an open or weakly closed ionization channel in the MQDT sense, both open- and closed-type basis functions must be included for that channel. On the other hand, only closed-type basis functions should be included for a channel to be treated as strongly closed. (See Refs. 10 and 14 for further discussion of this aspect.)

All matrix elements involve integrations only over the finite-reaction volume. The wave function of the escaping photoelectron outside the reaction volume is represented by linear combinations of regular and irregular Coulomb functions in each channel, as always in MQDT. This implies that the radius of the reaction volume must be large enough so that the exchange interaction between the two electrons can be neglected outside the reaction volume. Higher-order electric multipole interactions between the two electrons are also neglected in the outer region, whereby the potential seen by the outer electron is Coulombic to an excellent approximation.

In this study we have utilized a reaction volume boundary of $r_0=31$ a.u. This is roughly the smallest distance beyond which the $6p$ radial wave function can be neglected. This criterion is appropriate because $6pns$ is the highest channel we have included in our MQDT calculation as a weakly closed channel. Test calculations using the much larger boundary $r_0=43$ showed only minor differences in the final cross sections. Using a value of r_0 which is larger than necessary should be avoided if possible, of course, because it increases the number of basis functions needed to attain convergence.

A somewhat surprising result of our tests was the observation of a dependence of the short-range quantum defect matrix on r_0. This r_0 dependence of μ_{ij} was especially noticeable when a strongly closed channel was treated as weakly closed in the calculation. A similar r_0 dependence emerged in Ref. 27. Apparently it derives from the fact that treatment of a strongly closed channel as if it were a conventional MQDT weakly closed channel leads to exponential growth of that channel component even within the reaction volume. The variational R-matrix calculation would seem to be slightly unstable as a result, causing this undesirable r_0 dependence. Nevertheless, in all cases we considered, this r_0 dependence disappeared from all final results after the large-r boundary conditions were imposed by MQDT procedures. In particular the total and partial photoionization cross sections were always insensitive to r_0, implying that this apparent instability causes no practical difficulties.

The present calculation requires a substantially larger basis than the lower-energy calculations of papers I and II. Three factors account for this. First, there are simply more channels involved in this higher-energy range than at lower energies. For $E > -0.135$ a.u. there are 16 open or weakly closed channels, while in the previous work we had a maximum of five such channels in the $^1P^0$ calculation. Second, the two-electron wave functions containing one highly-excited electron orbital become much more important as the energy increases, primarily to represent the continuum of the lowest channels such as $4s\epsilon p$. These play a smaller role at low energies. Normally, the energy of the highest one-electron orbital in each channel should be well above the total energy at which the R-matrix calculation is desired. Finally, because of the larger boundary r_0, the density of Ca^+ bound states confined within the reaction volume is larger. While a maximum of seven closed-type one-electron radial functions for each l was sufficient in paper I, here it is necessary to use 10–12 closed-type radial functions for each l.

Increasing the number of basis functions further does not appreciably affect the final results but increases the computing time. In the final calculation we used 137 two-electron basis functions for the lowest subregion and 167 basis functions for the highest subregion.

We have no precise general criterion for choosing the number of basis functions to use in each channel. The eigenvectors of Eq. (2) provide some insight. We begin the calculation with a large basis, after which it is possible to eliminate basis functions whose contributions are clearly negligible. Note that the eigenvectors corresponding to different eigenvalues can be very different and that a basis function with a small component in one particular eigenvector may contribute significantly to other eigenvectors. Of course, the eigenvectors also depend on the energy E.

C. Interpolation of the MQDT parameters

As we stated above the short-range MQDT parameters are functions of the total energy. To obtain the fine details of the cross section it is necessary to use a fine energy mesh for the MQDT calculation. It is unpractical to perform the R-matrix calculation at every energy when a large number of basis functions are included. Thus it is imperative to obtain the short-range parameters on a coarse energy mesh and in the smoothest possible form, followed by interpolation when the MQDT calculation is performed on a fine energy mesh. The reaction matrix[16] K_{ij} might be a candidate for this interpolation, but its poles would require very careful treatment. A preferable choice is the set of eigenquantum defects μ_α and eigenvectors $U_{i\alpha}$ defined by the following equation:

$$K_{ij}=\sum_\alpha U_{i\alpha}\tan(\pi\mu_\alpha)(\mathbf{U}^T)_{\alpha j} \tag{3}$$

as these are normally expected to be smooth, slowly varying functions of E. (The superscript T denotes the matrix transpose.) As E approaches the double-escape threshold and as r_0 increases, however, the dimension of the short-range reaction matrix increases and its parameters acquire a more complicated energy dependence. With this growth in channel number the μ_α have numerous avoided crossings. These crossings pose particular difficulties when they are narrowly avoided as the $U_{i\alpha}$ change very rapidly in their vicinity. For this reason, the μ_α and $U_{i\alpha}$ do not seem to be the smoothest quantities to work with. The best choice we have found after some experimentation is the quantum-defect matrix μ_{ij}, defined as in paper I by

$$\mu_{ij}=\sum_\alpha U_{i\alpha}\mu_\alpha(\mathbf{U}^T)_{\alpha j}\ . \tag{4}$$

This matrix has no poles and its elements normally

remain smooth near avoided crossings of the μ_α. Knowledge of the μ_{ij} matrix is equivalent to knowledge of the K matrix, and μ_{ij} is better suited for interpolation. In the actual calculation, we obtain μ_α and $U_{i\alpha}$ by diagonalizing the K matrix at each selected energy. By connecting the appropriate branches of μ_α at each energy we obtain continuous eigenquantum defects μ_α as functions of energy. A smooth μ matrix is then constructed using Eq. (4).

The smoothness of the quantum-defect matrix depends to some extent on the branches chosen for the μ_α. Since they are only defined modulo 1 by Eq. (3) and μ_α can be shifted by an integer without affecting the reaction matrix. Such changes *do* affect the smoothness of μ_{ij}, though, as can be seen from Figs. 1 and 2 for an eight-channel calculation. With the choice of branches made in Fig. 1(a), an avoided crossing between $\alpha=1$ and $\alpha=8$ at $E=-0.208$ a.u. is less obvious than the corresponding avoided crossing between the lowest two curves in Fig. 1(b). These two sets of μ_α differ only in the branch of one curve, namely the highest curve in Fig. 1(a) and the lowest in Fig. 1(b). Figure 2 shows that the branch choice in Fig. 1(b) leads to a smoother quantum-defect matrix than that of Fig. 1(a). This is because two eigenquantum defects μ_α which have an avoided crossing should preferably be located on the same branch at the crossing, as this produces the smoothest possible μ_{ij} matrix. Clearly the quantum-defect matrix elements in Fig. 2(b) are better suited for interpolation than those of Fig. 2(a), and consequently the matrix elements in Fig. 2(b) require fewer energy mesh points. This is only a minor technical point concerning the interpolation. The final cross sections are not affected by such differences in the choice of branches in the μ_α, if enough energy mesh points are used.

D. MQDT calculations

For any MQDT calculation it is necessary to decide which channels should be treated as open or weakly closed in each energy region. The choice is not very critical in the sense that fairly consistent results can be obtained using different numbers of channels. Note that the choice of channels to be included as weakly closed channels must be decided before the R-matrix calculation is performed, as we must include in the variational basis some open-type basis functions for those weakly closed channels as well as for all open channels. (See Sec. II B.)

As an approximate rule of thumb, a specific channel (e.g., $5p\epsilon d$) is treated as strongly closed at energies well below the lowest resonant state ($5p5d$) in that channel. At higher energies it is normally treated as weakly closed. To treat a channel as strongly closed means that this channel is not included in the MQDT calculation. However, each resonance of this channel will still show up correctly in the photoionization cross section if the "bound portion" of the corresponding two-electron wave function fits entirely into the volume defined by the boundary r_0. It is also essential to have appropriate basis functions in the R-matrix calculation.

Including strongly closed channels by treating them as weakly closed MQDT channels does not affect the final cross sections or other observables, but it complicates the calculation by causing additional avoided crossings of the μ_α and a generally stronger energy dependence of the μ_α. This also causes near degeneracies of the μ_α associated with the strongly closed channels. Inclusion of too-few channels, i.e., failure to include all weakly closed channels, on the other hand, will distort the final results. In

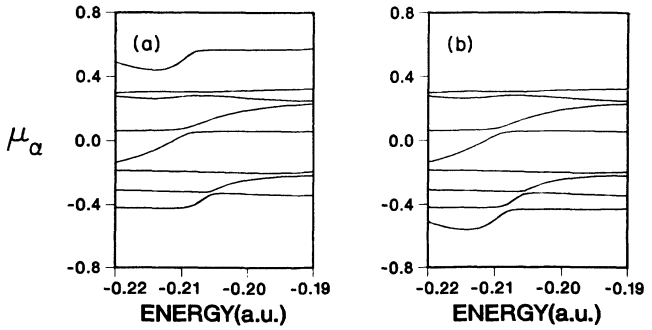

FIG. 1. Eigenquantum defects μ_α are shown as functions of the total energy E. (a) Smooth μ_α obtained from an eight-channel calculation. Note the avoided crossing between the lowest and the highest curves. (b) μ_α obtained by subtracting 1 from the uppermost μ_α at all energies. Now there is no avoided crossing between the highest and the lowest μ_α.

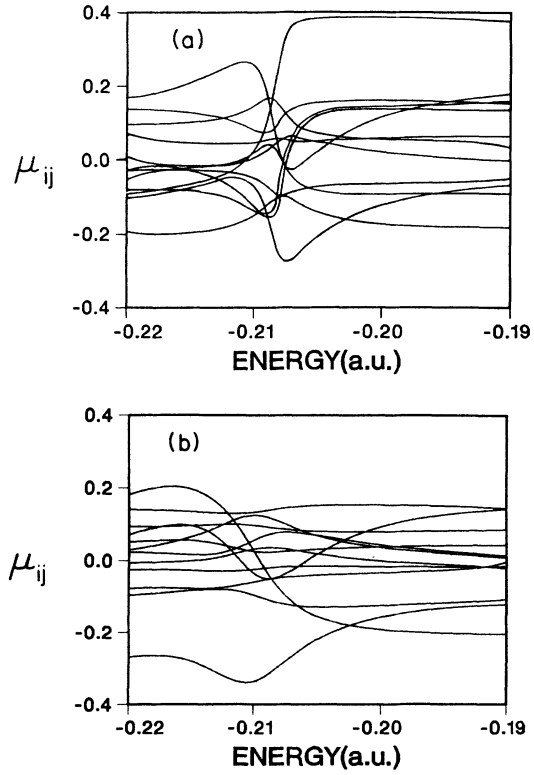

FIG. 2. Dependence of the quantum-defect matrices μ_{ij} on the branch chosen for the μ_α. (a) Some elements of the μ_{ij} obtained with the μ_α of Fig. 1(a); (b) the same elements obtained with the μ_α of Fig. 1(b).

particular, resonances in the omitted channels will lie much too high in energy unless the wave functions representing these channels fit into the box defined by the boundary r_0. In Fig. 3 we show a comparison of three calculations performed using different numbers of channels. The μ_α and the photoionization cross sections are shown for each calculation. Figures 3(a) and 3(b) show an eight-channel calculation which includes five open channels ($4s\epsilon p$, $3d\epsilon p$, $3d\epsilon f$, $4p\epsilon s$, and $4p\epsilon d$) and three weakly closed channels ($5s\epsilon p$, $4d\epsilon p$, and $5p\epsilon s$). A ten-channel calculation including two more weakly closed channels ($4d\epsilon f$ and $5p\epsilon d$) is shown in Figs. 3(c) and 3(d). Finally a 16-channel calculation treating six more channels ($4f\epsilon d$, $4f\epsilon g$, $6s\epsilon p$, $5d\epsilon p$, $5d\epsilon f$, and $5p\epsilon s$) is shown in Figs. 3(e) and 3(f). The ten-channel calculation has included all weakly closed channels in the energy range. The six additional channels treated as weakly closed channels in the 16-channel calculation *are actually strongly closed* for the energy considered. The two calculations [see Figs. 3(d) and 3(f)] show no significant difference in the final cross sections, whereas several differences between the eight-channel and the ten-channel result are quite obvious. This is because the two weakly closed channels $4d\epsilon f$ and $5p\epsilon d$ have resonances which are pushed above this energy range in the eight-channel calculation since they do not fit inside the R-matrix box. The ten-channel calculation therefore seems to be the best choice. Compared to the ten-channel calculation, both the eight- and 16-channel calculations show [see Figs. 3(a), 3(c), and 3(e)] strong energy dependences of the μ_α, and their avoided crossings are narrower and more severe. Figure 3(e) also shows near degeneracies among some of the μ_α associated with the strongly closed channels. These strong energy dependences and avoided crossings show up in the quantum defect matrix μ_{ij} as well, making it more difficult to perform the interpolation. In fact, for the eight- and 16-channel calculations it was necessary to calculate the R matrix by solving Eq. (1) on a much smaller energy mesh.

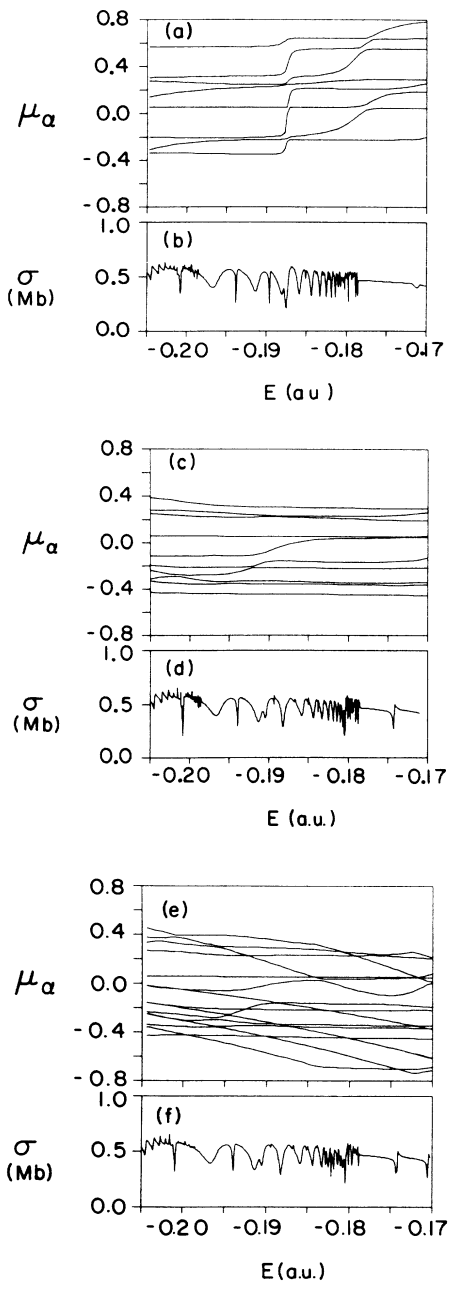

FIG. 3. Comparisons of μ_α and photoionization cross sections obtained from (a), (b) eight-channel calculation; (c), (d) ten-channel calculation (e), (f) 16-channel calculation.

E. S matrix

The short-range scattering matrix is

$$S_{ij} = \sum_\alpha U_{i\alpha} \exp(2i\pi\mu_\alpha)(\mathbf{U}^T)_{\alpha j} \ . \tag{5}$$

This can be interpreted as the quantum-mechanical amplitude that an electron which collides with the target ion (Ca^+) in channel j will recoil from the ion in channel i. It is not, however, the physical scattering matrix which connects only the open channels. This S matrix is constructed from the reaction matrix and does not incorporate any boundary conditions at $r \to \infty$, whereby it normally remains a smooth function of energy and does not display resonance effects associated with weakly closed channels. Equation (5) is clearly symmetric. The diagonal elements $|S_{ii}|^2$ represent the probability that an electron remains in the same channel after colliding with the ionic core. The off-diagonal elements $|S_{ij}|^2$ provide an index of the mixing of channels i and j. By examining elements of $|S_{ij}|^2$ as functions of the total energy, we see how the interaction between successive channels "turns on" as the total energy increases.

F. Resonances and the wave functions at the resonances

One of the purposes of this work is to classify the high-lying resonance series. Positions of resonances are not always easily extracted from the photoionization spectra, and some resonances fail to show up in the cross section. The energies at which resonances occur can be determined by the following equation:[16,33]

$$\det | \bar{U}_{i\alpha}(E)\sin[\beta_i(E)+\pi\bar{\mu}_\alpha(E)] | =0 , \quad (6)$$

where $\beta_i=\pi[-2(E-E_i)]^{-1/2}$, E_i being the threshold energy of the ith channel. The $\bar{U}_{i\alpha}$ and $\tan\pi\bar{\mu}_\alpha$ are the eigenvector matrix and the eigenvalues of the closed portion of the original K matrix obtained by eliminating all the open channels. The distribution of the bound portion of the wave function among the weakly closed channels at a resonance energy is determined by[33]

$$Z_i=N^{-1}\nu_i^{3/2}(-1)^{l_i+1}\sum_\alpha \bar{U}_{i\alpha}\cos(\beta_i+\pi\bar{\mu}_\alpha)A_\alpha , \quad (7)$$

where A_α is a solution of the following equation:

$$\sum_\alpha \bar{U}_{i\alpha}\sin(\beta_i+\pi\bar{\mu}_\alpha)A_\alpha=0 \quad (8)$$

and N is a normalization constant. These amplitudes Z_i can be used to determine the dominant channel i to which a resonance belongs.

III. RESULTS

A. Photoionization spectra

Figure 4 shows our theoretical prediction for the calcium photoionization cross section for final-state energies between -0.32 and -0.12 a.u. The corresponding photon wavelength can be obtained by using the experimental ground-state energy $E_g=-0.6609$ a.u. Note that the energy scale in Fig. 4(a) is twice as large as that of 4(b) and 4(c). In Figs. 4(a) and 4(c) the upper curves are velocity results and the lower ones are length results. Figure 4(b) shows only the velocity results for clarity. The velocity result and the length result show almost exactly the same pattern throughout the energy range except for energies above the $4f$ threshold where the two forms begin to have significantly different shapes, showing that our calculation is deteriorating in accuracy. The length form of the cross section is about 10–25 % lower than the velocity form over most of the spectrum. This difference is rather large compared to the low-energy region studied in papers I and II.

Different numbers of channels are used for each subregion. Table I displays the channels included in each energy region. Naturally, all of the open channels are included. More and more weakly closed channels are also included as the energy increases. As we stated above, a new channel is added when the energy is about to reach the first resonance energy of that series. In test calculations near $E=-0.21$ a.u. we have experimented with anywhere from 9 to 17 channels, including varying numbers of strongly closed channels (treated as weakly closed) as well. The differences in the cross section were always very small despite vast differences in the μ_{ij} matrix and in

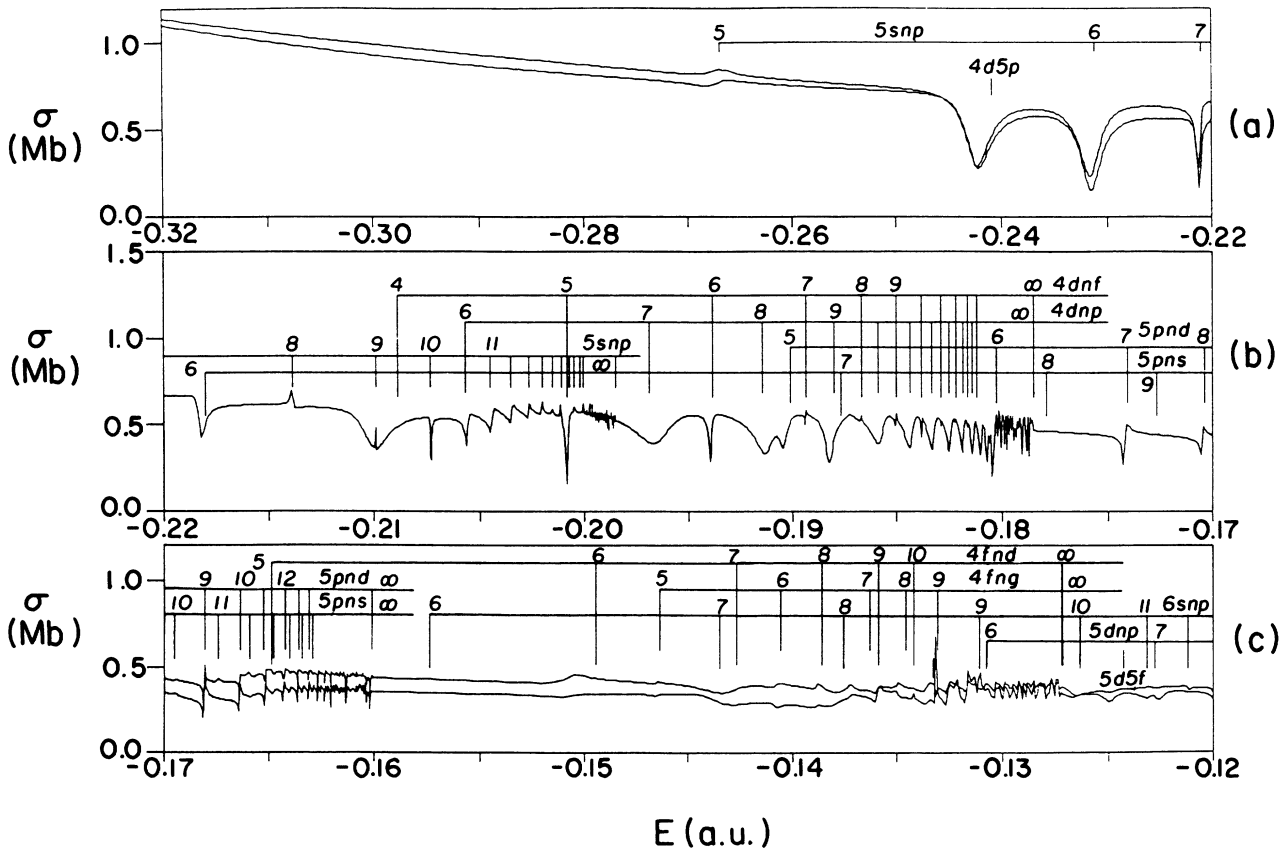

FIG. 4. Theoretical photoionization spectra of calcium atom in LS coupling. (a) For E between -0.32 and -0.22; (b) for E between -0.22 and -0.17; (c) for E between -0.17 and -0.12. Note the different energy scale of (a). (a) and (c) The upper curve is the velocity result, and the lower curve is the length result.

TABLE I. Ionization channels included in the MQDT calculations. Items listed in the third column are the channels added to the energy region in addition to the channels already included in the preceding subregion.

Energy (a.u.)	Number of channels	Channels added
$-0.32 \sim -0.28$	5	$4s\epsilon p, 3d\epsilon p, 3d\epsilon f, 4p\epsilon s, 4p\epsilon d$
$-0.28 \sim -0.25$	6	$5s\epsilon p$
$-0.25 \sim -0.22$	7	$4d\epsilon p$
$-0.22 \sim -0.20$	9	$4d\epsilon f, 5p\epsilon s$
$-0.20 \sim -0.17$	10	$5p\epsilon d$
$-0.17 \sim -0.15$	12	$4f\epsilon d, 6s\epsilon p$
$-0.15 \sim -0.135$	13	$4f\epsilon g$
$-0.135 \sim -0.12$	16	$5d\epsilon p, 5d\epsilon f, 6p\epsilon s$

the μ_α. Note that two-electron basis functions representing strongly closed channels must be included in the R-matrix calculation as in papers I and II.

We have attempted to identify all the resonances in this energy range, including several which are hardly evident in the photoionization cross section of the ground state. Because of strong mixing among channels it is not always meaningful to label a resonance with the quantum numbers of independent-particle states. For example, the states $4d5p$ and $5s6p$ are almost equally mixed with each other. We used Eq. (6) to find the "position" of each resonance, which is normally adequate to locate the resonance position with an error comparable to its autoionization width. At each resonance energy, Eq. (7) helps to identify the dominant channel, though in some cases it is not necessarily the channel having the maximum Z_i. At energies near a threshold, the effective principal quantum numbers of successive levels in a resonance series are separated by an integer except near perturbing energy levels from other channels. Analysis of a Lu-Fano plot can also be used to identify some resonances. Despite the use of all these methods, it was still very difficult to classify all resonances with proper labels. In any case the labels given to resonances in this work should not be taken too seriously.

The cross section exhibits a variety of profiles in different energy regions. Just above the $4p$ threshold, the cross sections are featureless until the $5s5p$ resonance occurs. The absence of resonances for a wide range below $5s5p$ relates to the relatively large gap between the $4p$ and $5s$ threshold energies (about 0.13 a.u.) causing the $5s5p$ resonance to lie well above the $4p$ threshold. The surprisingly small $5s5p$ resonance is followed by the first resonance of the $4dnp$ series (namely, $4d5p$) which is in turn followed by $5s6p$ and $5s7p$. These three resonances are much stronger than $5s5p$ apparently because of borrowed strength from $4d5p$. At these energies the $4d5p$ and $5s6p$ have nearly equal mixing. As the energy increases [see Fig. 4(b)], we reach the $5p6s$ resonance. Owing to the strong interactions among the $5snp$, $4dnp$, and $5pns$ channels, the spectrum appears somewhat unusual, with line shapes varying from one resonance to the next. As the energy approaches the $5s$ threshold, the $5snp$ resonance series shows a regular high-n Rydberg behavior. These resonances would be uniformly spaced on an effective quantum number scale $(-\epsilon)^{-1/2}$. The three interlopers $4d4f$, $4d6p$, and $4d5f$ cause the $5snp$ series to deviate from an otherwise regular distribution. Each threshold is marked in the figure as $n=\infty$.

Above the $5s$ threshold, the dominant features are the $4dnf$ and $4dnp$ series. They are perturbed strongly by $5p5d$, $5p7s$, and $5p6d$. The spectra between the $4d$ and the $5p$ thresholds consist primarily of $5pnd$ and $5pns$ resonances. The lowest four resonances of these two series are below the $4d$ threshold. Above the $4d$ threshold the only interloper is the $4f5d$ resonance at $E=-0.165$. The $6s6p$ resonance does not give any noticeable feature in the cross section, even more surprising than the weak $5s5p$ resonance.

B. S matrix

The absolute squares of elements of the S matrix are shown in Fig. 5 as functions of energy. The S matrix used here is taken from a separate ten-channel calculation covering an energy range from $E=-0.23$ to $E=-0.17$. In each figure, the value of each element $|S_{ij}|^2$ is represented by the height of a vertical bar. The horizontal axes are labelled by the appropriate ionization channels. Diagonal elements represent the probability that an electron remains in the same channel after colliding with the core, while off-diagonal elements measure the strength of interaction between any two channels. For an energy at which a particular channel i is strongly closed, the corresponding diagonal element $|S_{ii}|^2$ is very close to 1, indicating that only elastic scattering is possible through this channel. Electrons from other channels cannot get into this energetically forbidden channel. All off-diagonal elements connecting to this channel are very small. When the energy increases so that this channel becomes weakly closed, the size of its diagonal element is reduced and the off-diagonal elements connecting to this channel begin to grow.

Consider first the scattering probabilities connecting the first five channels, $4s\epsilon p$, $3d\epsilon p$, $3d\epsilon f$, $4p\epsilon s$, and $4p\epsilon d$ only. These are shown in the lower-left corner of each picture in Fig. 5. This portion of $|S_{ij}|^2$ does not change much with energy, because each of these five channels has already been open at much lower energies and the interactions among them are hardly affected by new channels. Note the exceptionally large scattering probability connecting the $3d\epsilon f$ and the $4p\epsilon d$ channels, nearly 70%. The interaction between these two channels was seen in paper I to become strong already at energies below the $3d$ threshold. Similarly, the pairs of channels $3d\epsilon p$-$4s\epsilon p$ and $4p\epsilon d$-$3d\epsilon p$ are strongly mixed. Our present results connect smoothly with the results obtained at low energies in paper I, although the value of the boundary r_0 is very different for the two calculations (as is the number of channels).

Now consider the portion of the S matrix connecting the remaining five channels to each other, i.e., $5s\epsilon p$, $4d\epsilon p$, $4d\epsilon f$, $5p\epsilon s$, and $5p\epsilon d$. This part of the S matrix is shown in the upper-right corner of each figure. At low energy [Fig. 5(a)] all elements except those on the diago-

nal are very small. The energy is far below the point where the interaction between these channels "turns on" and still further below the thresholds where these channels become open. This proximity of the diagonal elements to unity indicates that these channels are strongly closed. As the total energy increases [see Figs. 5(b) and 5(c)] we see the off-diagonal elements becoming nonnegligible, as channel interactions grow. The size of the diagonal elements are reduced accordingly. In Fig. 5(b) the diagonal elements remain fairly large while in Fig. 5(c) they are all reduced significantly except for the element corresponding to the $5p\epsilon d$ channel. At $E=-0.17$ [see Fig. 5(d)] the $5s\epsilon p$, $4d\epsilon p$, and $4d\epsilon f$ channels are open. The $5p\epsilon s$ and $5p\epsilon d$ are weakly closed. Strong interactions are established among different channels. There is no longer a large-amplitude diagonal element. As for the interactions between the first five channels and the second five channels, we find that they are generally weak compared to the interaction within each group though they also grow slowly as the energy increases. We expect that this near-block diagonality of channel-interaction strength is a general feature, present to some extent in all systems.

C. Wannier resonance series

To predict energy positions for still higher-lying Wannier-ridge states up to $11s11p$, we have used the standard method of diagonalizing the two-electron Hamiltonian in a discrete basis, all of whose orbitals vanish at a finite boundary $r_0=120$ a.u. By inspecting the resulting eigenvectors the ridge states can be located in the eigenvalue spectrum with reasonably good certainty. Previous studies have shown that the total energy of such states satisfies a two-electron Rydberg formula[18–20] of the form (in a.u.):

$$E=-\frac{4(Z-\frac{1}{4}-\sigma)^2}{(n+\frac{3}{2}-\mu)^2}\ . \tag{9}$$

Here Z is the charge of the residual ionic core, in this case $Z=2$, while the principal quantum number n takes on positive integer values. The quantum defect μ is an unknown constant dependent on specific interactions between the electron pair and the ionic core. Finally σ is an effective screening parameter. Molina[34] has shown σ to have the following Z dependence for an electron pair

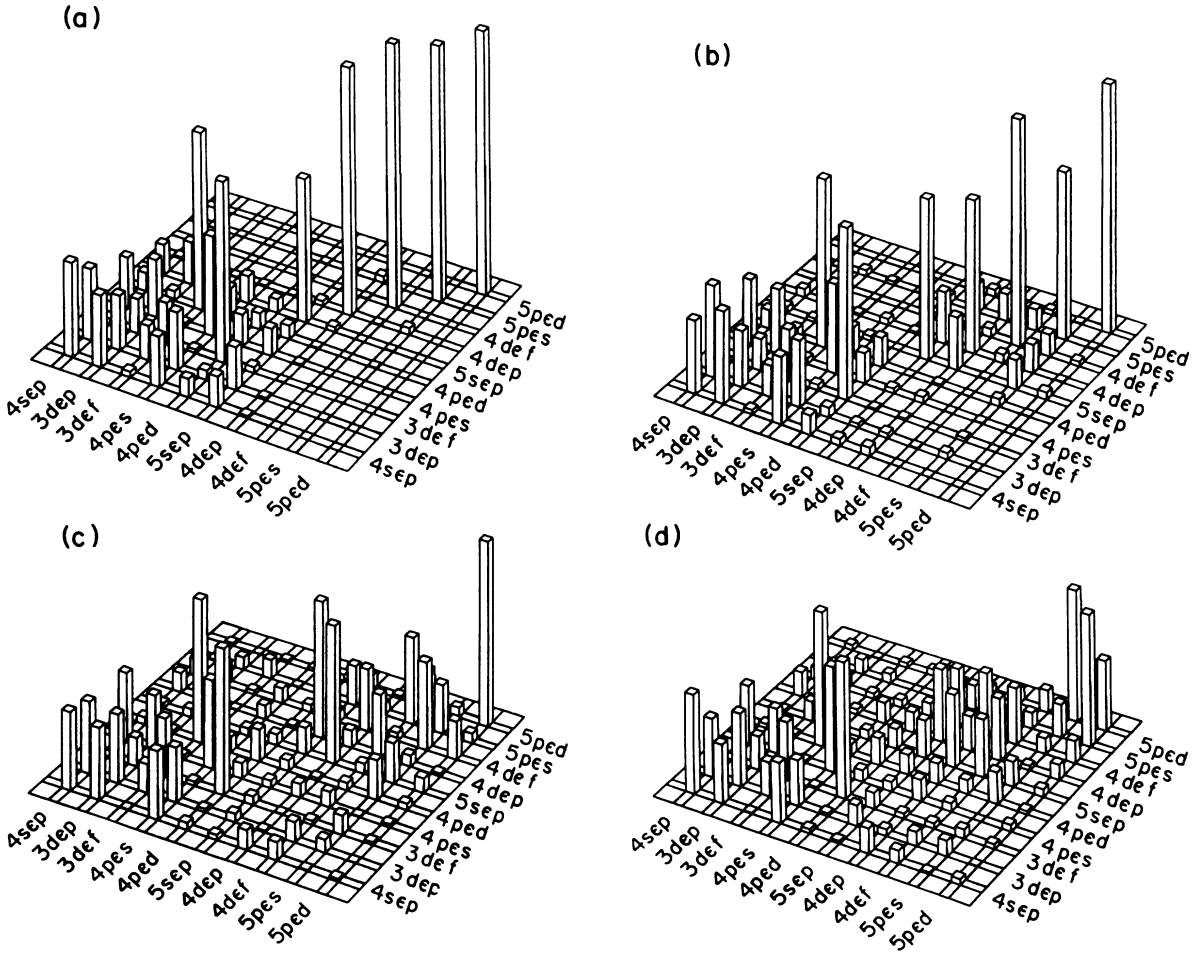

FIG. 5. Squared S-matrix elements for several selected energies. (a) For $E=-0.227$; (b) for $E=-0.215$; (c) for $E=-0.202$; (d) for $E=-0.17$. Each figure has the same scale. The highest peak of (a) has unit height. Note the general increase of channel-interaction strength and the decrease of diagonal elements with increasing energy.

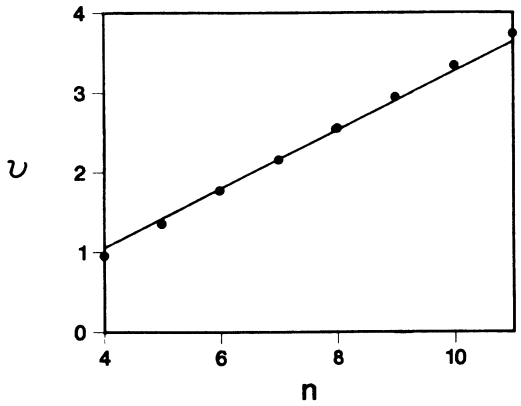

FIG. 6. Effective quantum numbers of *nsnp* energy levels of calcium atom. The calculated values are marked by solid circles. The straight line is from the two-electron Rydberg formula [Eqs. (9) and (10)] with the quantum defect μ fitted to the calculated value at $n=7$.

moving in the field of a point nucleus of charge Z:

$$\sigma = Z/2 - 0.166 - (2Z)^{1/2}/50 \ . \tag{10}$$

The applicability of Eqs. (9) and (10) to calcium *nsnp* levels can be tested by plotting our calculated energy levels on an effective quantum number scale, i.e., $\nu = (-2E)^{-1/2}$. This plot of ν versus n should then be a straight line with slope $[2\sqrt{2}(Z - \frac{1}{4} - \sigma)]^{-1}$. The calculated levels in Fig. 6 clearly do lie on a straight line. Moreover, the slope is reasonably close to the value expected for helium ($Z=2$) on the basis of Eqs. (9) and (10), differing by about 8%. It is not clear at present whether this difference is related to a fundamental difference between calcium and helium, such as the nondegeneracy of $Ca^+(nl)$ levels, or whether it derives from inaccuracies in the calculation. Experimental efforts should help to decide this matter, although the weak nature of $5s5p$ and $6s6p$ suggests that these ridge states will be difficult to observe.

IV. CONCLUSION

The present paper and the earlier papers I and II have shown that the complex photoabsorption spectra of atomic calcium are generally well described by eigenchannel R-matrix methods combined with MQDT. This includes the nonperturbative channel interactions reflecting strong correlations between the valence electrons, considered in I and the present paper (paper III), and the conspicuous spin-orbit effects described by a frame transformation in II. Comparable success is anticipated for the other partial waves relevant to e-Ca^+ scattering processes, though we have not explored these other symmetries in detail.

We have shown in this paper that it is possible to push the technology to deal with the larger reaction (volumes ($r_0 = 30-50$ a.u.) and larger numbers of channels (10–20) relevant at higher energies, but the practical difficulties grow rapidly with the energy. The difficulties involved in extending this analysis to still heavier open-shell atoms like the transition metals remain to be assessed.

A surprisingly large fraction of the present effort has been spent just in classifying and interpreting the calculated photoionization spectrum of Fig. 4. In fact this was more time consuming than the R-matrix and MQDT calculations themselves. Analysis of the relevant hyperspherical potential curves, such as those calculated in Ref. 25, would presumably simplify the interpretation procedure greatly. A hyperspherical analysis would also indicate at a glance the main channels that are strongly mixed. It should be pointed out, though, that the determination of hyperspherical potential curves at the high energies treated here requires a nontrivial computational effort in its own right. Such an analysis is recommended for subsequent studies of this energy range in calcium or in the other alkaline earths.

ACKNOWLEDGMENTS

This work was supported in part by the National Science Foundation. We thank Q. Molina for providing access to unpublished results.

[1]G. H. Newsom, Proc. Phys. Soc. London **87**, 975 (1966).
[2]T. J. McIlrath and R. J. Sandeman, J. Phys. B **5**, L217 (1972).
[3]J. P. Connerade, M. A. Baig, W. R. S. Garton, and G. H. Newsom, Proc. R. Soc. London, Ser. A **371**, 295 (1980).
[4]Z. Altun, S. L. Carter, and H. P. Kelly, J. Phys. B **15**, L709 (1982); Phys. Rev. A **27**, 1943 (1983).
[5]P. Scott, A. E. Kingston, and A. Hibbert, J. Phys. B **16**, 3945 (1983).
[6]N. Karamatskos, M. Mueller, M. Schmidt, and P. Zimmermann, J. Phys. B **18**, L107 (1985).
[7]K. C. Pandey, S. S. Jha, and J. A. Armstrong, Phys. Rev. Lett. **44**, 1583 (1980); J. A. Armstrong, S. S. Jha, and K. C. Pandey, Phys. Rev. A **23**, 2761 (1981).
[8]K. Ueda, Phys. Rev. A **35**, 2484 (1987).
[9]U. Griesmann, N. Shen, J. P. Connerade, K. Sommer, and J. Hormes, J. Phys. B **21**, L83 (1988).
[10]C. H. Greene and Longhuan Kim, Phys. Rev. A **36**, 2706 (1987).
[11]Longhuan Kim and C. H. Greene, Phys. Rev. A **36**, 4272 (1987).
[12]U. Fano and C. M. Lee, Phys. Rev. Lett. **31**, 1573 (1973).
[13]H. Le Rouzo and G. Raseev, Phys. Rev. A **29**, 1214 (1984).
[14]C. H. Greene, Phys. Rev. A **28**, 2209 (1983); **32**, 1880 (1985); J. Opt. Soc. Am. B **4**, 775 (1987); C. H. Greene, in *Fundamental Process of Atomic Dynamics*, edited by J. Briggs, H. Kleinpoppen, and H. Lutz (Plenum, New York, 1988).
[15]M. J. Seaton, Rep. Prog. Phys. **46**, 97 (1983).
[16]U. Fano and A. R. P. Rau, *Atomic Collisions and Spectra* (Academic, Orlando, 1986).
[17]C. H. Greene and Ch. Jungen, Adv. At. Mol. Phys. **21**, 51

(1985).
[18]F. H. Read, J. Phys. B **10**, 449 (1977); S. J. Buckman, P. Hammond, F. H. Read, and G. C. King, *ibid.* **16**, 4219 (1983).
[19]A. R. P. Rau, J. Phys. B **16**, L699 (1983).
[20]C. D. Lin and S. Watanabe, Phys. Rev. A **35**, 4499 (1987).
[21]J. W. Cooper, U. Fano, and F. Prats, Phys. Rev. Lett. **10**, 518 (1963).
[22]R. P. Madden and K. Codling, Astrophys. J. **141**, 364 (1965).
[23]P. R. Woodruff and J. A. R. Samson, Phys. Rev. A **25**, 848 (1982).
[24]J. Dubau and J. Wells, J. Phys. B **6**, 1452 (1973); G. N. Bates and P. L. Altick, *ibid.* **6**, 653 (1973); V. Radojevic and W. R. Johnson, Phys. Rev. A **31**, 2991 (1985).
[25]C. H. Greene, Phys. Rev. A **23**, 661 (1981).
[26]P. F. O'Mahony and C. H. Greene, Phys. Rev. A **31**, 250 (1985).
[27]M. Aymar, E. Luc-Koening, and S. Watanabe, J. Phys. B **20**, 4325 (1987); M. Aymar, *ibid.* **20**, 6507 (1987).
[28]M. Aymar, Phys. Rep. **110**, 163 (1984).
[29]J. A. Armstrong, J. J. Wynne, and P. Esherick, J. Opt. Soc. Am. **69**, 211 (1979); J. A. Armstrong, P. Esherick, and J. J. Wynne, Phys. Rev. A **15**, 180 (1977).
[30]J. J. Wynne and J. A. Armstrong, Comments At. Mol. Phys. **8**, 155 (1979).
[31]J. P. Desclaux, Comput. Phys. Commun. **1**, 216 (1969).
[32]K. Bartschat, M. R. H. Rudge, and P. Scott, J. Phys. B **19**, 2469 (1986).
[33]C. M. Lee and K. T. Lu, Phys. Rev. A **8**, 1241 (1973).
[34]Q. Molina (unpublished).